AIP | Applied Physics Letters

Temperature dependent optical properties of CH3NH3PbI3 perovskite by spectroscopic ellipsometry

Yajie Jiang, Arman Mahboubi Soufiani, Angus Gentle, Fuzhi Huang, Anita Ho-Baillie, and Martin A. Green

Citation: Applied Physics Letters **108**, 061905 (2016); doi: 10.1063/1.4941710
View online: http://dx.doi.org/10.1063/1.4941710
View Table of Contents: http://scitation.aip.org/content/aip/journal/apl/108/6?ver=pdfcov
Published by the AIP Publishing

Temperature dependent optical properties of $CH_3NH_3PbI_3$ perovskite by spectroscopic ellipsometry

Yajie Jiang,[1,a)] Arman Mahboubi Soufiani,[1] Angus Gentle,[2] Fuzhi Huang,[3] Anita Ho-Baillie,[1] and Martin A. Green[1]

[1]*Australian Centre for Advanced Photovoltaics, School of Photovoltaic and Renewable Energy Engineering, UNSW Australia, Sydney 2052, Australia*

[2]*School of Mathematical and Physical Sciences, University of Technology Sydney, PO Box 123, Broadway, 2007 NSW, Australia*

[3]*State Key Laboratory of Advanced Technology for Materials Synthesis and Processing, Wuhan University of Technology, Wuhan 430070, China*

(Received 3 December 2015; accepted 28 January 2016; published online 10 February 2016)

Mixed organic-inorganic halide perovskites have emerged as a promising new class of semiconductors for photovoltaics with excellent light harvesting properties. Thorough understanding of the optical properties of these materials is important for photovoltaic device optimization and the insight this provides for the knowledge of energy band structures. Here we present an investigation of the sub-room temperature dependent optical properties of polycrystalline thin films of $CH_3NH_3PbI_3$ perovskites that are of increasing interest for photovoltaics. The complex dielectric function of $CH_3NH_3PbI_3$ in the energy range of 0.5–4.1 eV is determined between 77 K and 297 K using spectroscopic ellipsometry. An increase in optical permittivity as the temperature decreases is illustrated for $CH_3NH_3PbI_3$. Optical transitions and critical points were analyzed using the energy dependent second derivative of these dielectric functions as a function of temperature. © *2016 AIP Publishing LLC*. [http://dx.doi.org/10.1063/1.4941710]

In recent years, mixed organic-inorganic halide perovskites have demonstrated great potential as a material for low-cost, high-efficiency thin film photovoltaics owing to their excellent light harvesting[1–4] and transport properties.[5–8] Comprehensive studies of the optical properties of these materials are needed for establishing robust optical models to improve the design of solar cells. The cubic-tetragonal-orthorhombic phase transition of $CH_3NH_3PbI_3$ perovskite has been systematically investigated by Calorimetric and IR spectroscopy[9] as well as single crystal/powder X-ray diffraction.[10,11] $CH_3NH_3PbI_3$ undergoes a phase transition from cubic to tetragonal at circa 330 K, and it forms an orthorhombic structure below approximately 160 K. The complex refractive index of $CH_3NH_3PbI_{3-x}Cl_x$ and $CH_3NH_3PbI_3$ perovskite films have been reported by many groups recently.[12–20] Temperature dependent dielectric constants of $CH_3NH_3PbX_3$ (X = I, Br, Cl) were determined at microwave frequencies (50, 90, and 150 GHz) by Poglitsch and Weber,[21] showing a discontinuity in the complex permittivity of all the halides at the orthorhombic/tetragonal phase transition, while no apparent changes were observed for the tetragonal/cubic transition. Similar behaviour was found by Onoda-Yamamuro *et al.*[22] for frequencies between 20 Hz and 1 MHz. These observations were attributed to the methylammonium cations being fully ordered in the orthorhombic phase, while disordered in the tetragonal and cubic phases. The absence of dramatic changes in optical properties across the tetragonal to cubic transition could be attributed to the large sub-picosecond structural fluctuations at high temperature phase,[23] equivalent to optical transition timescales. It is necessary to study the corresponding optical properties of $CH_3NH_3PbI_3$ in the visible/near infrared region with their increasing relevance for photovoltaic device design. This work differs from previous work as it studies the temperature dependent dielectric functions of $CH_3NH_3PbI_3$ determined at a wider energy range of 0.5–4 eV by spectroscopic ellipsometry from room temperature (RT) down to 77 K. Energy transitions as well as interband critical points (CPs) are also investigated by analysing second derivative spectra.

$CH_3NH_3PbI_3$ films were deposited on clean thin (1 mm thick) microscope glass substrates using the gas-assisted technique.[24] In brief, 25 μl 45 wt. % $CH_3NH_3PbI_3$ dimethylformamide (DMF) solution, prepared from PbI_2 and CH_3NH_3I in a molar ratio of 1:1, was spread on the substrate, then spun at 6500 rpm. After 2 s a dry argon gas was blown on the substrate whilst spinning. The sample was then annealed at 100 °C.

A J. A. Woollam V-VASE Ellipsometer with a Janis Research Model ST-400 UHV Supertran cryostat system attached utilising liquid nitrogen cooling was used to measure the temperature dependence of the films. Prior to attaching the cryostat the samples were measured in air at 65° and 70° incidents to establish an optical model for the room temperature optical properties.

Delta offset corrections for the cryostat windows were determined using the manufacturer's standard routine using a 20 nm thick thermal oxide on silicon wafer and calibrated for multiple angles. To remove any backside reflection from the glass substrate, which interferes with the window offset delta correction, the glass samples had the rear surface carefully roughened via sandblasting.

The dielectric function was determined by modelling using the computer software WVASE®, with two Psemi-Triangle (PSTRI) oscillators[25] at fundamental bandgaps around 1.6 eV and 2.8 eV appropriately describing the optical

[a)]Author to whom correspondence should be addressed. Electronic mail: yajie.jiang@unsw.edu.au

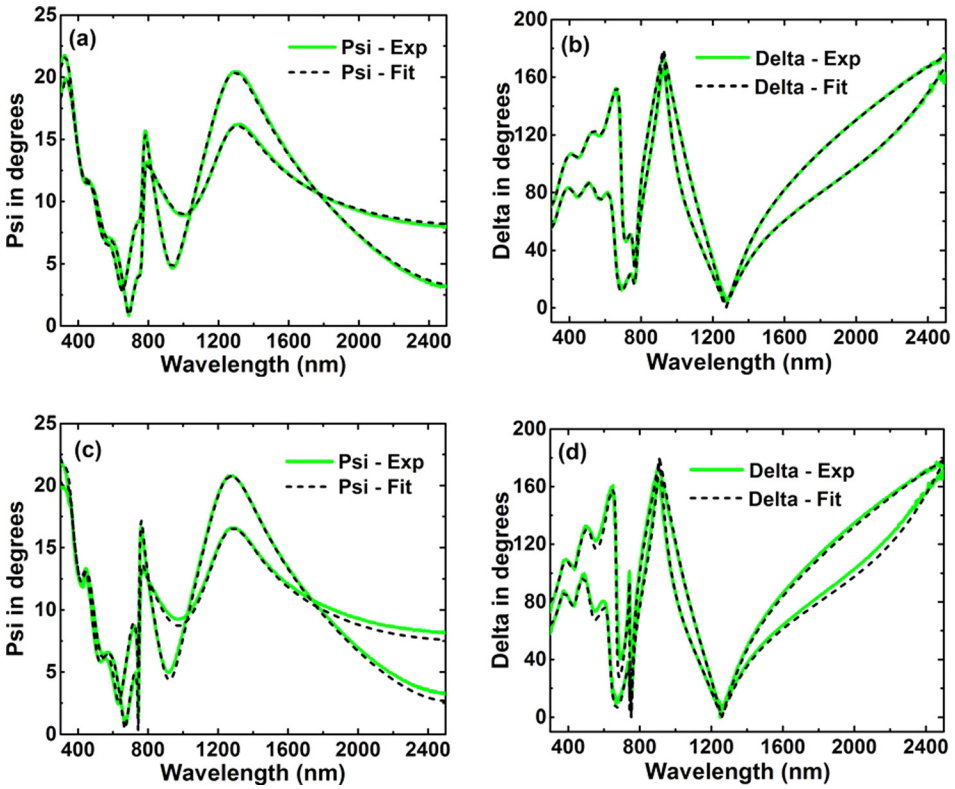

FIG. 1. Modelled (black dashed lines) and experimental (green solid lines) (a), (c) amplitude component Ψ and (b), (d) phase difference Δ of a $CH_3NH_3PbI_3$ perovskite film deposited on glass substrate. The ellipsometry data are collected at (a), (b) room temperature and (c), (d) 77 K for two incident angles 67° and 70°.

transitions. Gaussian oscillators were used to model the remaining regions of the spectrum. Details are described in Refs. 17 and 18. Figure 1 show the fits to experimental amplitude component Ψ and phase difference Δ of the polarized reflected light from the surface of a $CH_3NH_3PbI_3$ perovskite film deposited on a thin glass substrate at RT and 77 K. $CH_3NH_3PbI_3$ perovskite film thickness was determined to be 260 nm with 46 nm surface roughness and 7% void at room temperature, and the same structural parameters were used for all the lower temperature modeling's. An almost perfect match between the experimental and simulated data was achieved. Fittings to the other temperatures are given in the supplementary material.[26]

Dynamic ellipsometry data were also collected under continuous cooling and heating to investigate the optical properties over the phase transition regions. The sample was first cooled down *in-situ* from room temperature to 77 K, and subsequently heated up to room temperature again at a rate of 1.6 K/min. As

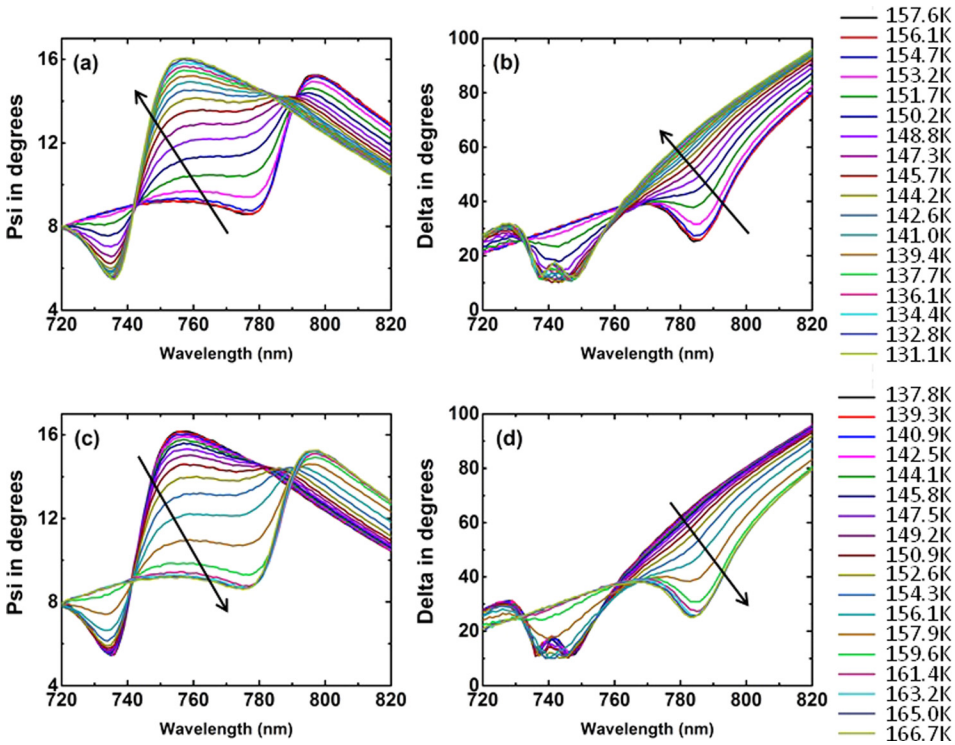

FIG. 2. Evolution of experimental ellipsometry data during (a), (b) cooling and (c), (d) heating process in 720–820 nm wavelength range. The ellipsometry data are collected for an incident angle of 70°.

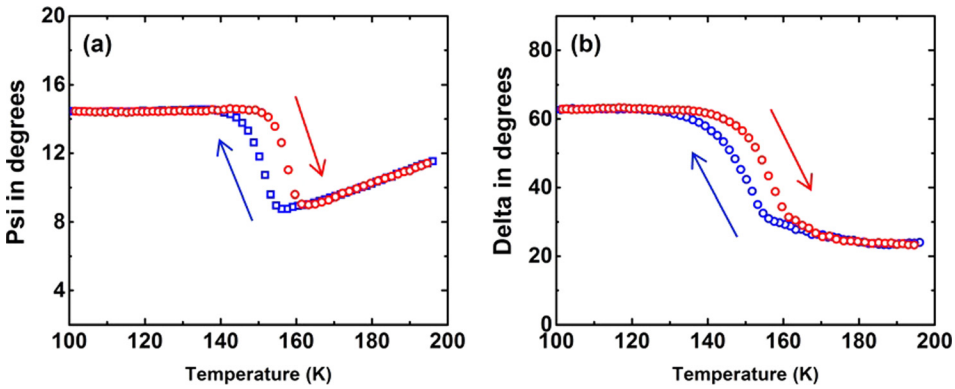

FIG. 3. Experimental (a) Psi and (b) Delta values recorded at 1.59 eV photon energy (780 nm) while cooling the sample from 200 K to 100 K (blue squares) and while subsequently heating the sample from 100 K to 200 K (red circles). The ellipsometry data are collected for an incident angle of 70°. The heating and cooling rate was set at 1.6 K/min.

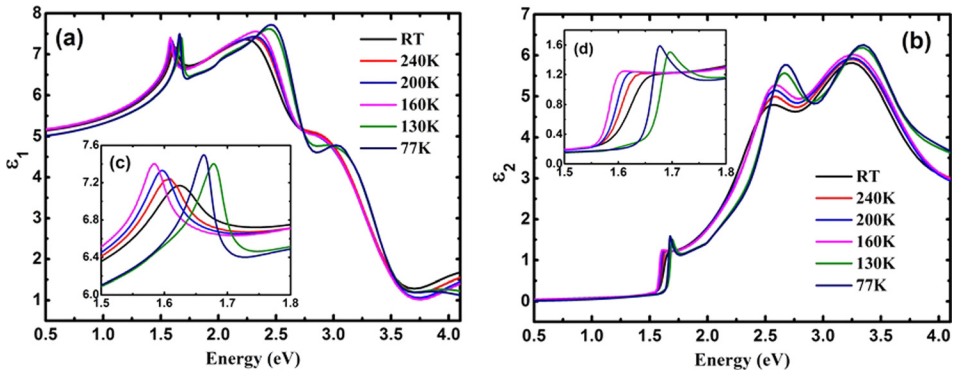

FIG. 4. (a) Real and (b) imaginary part of the dielectric function of $CH_3NH_3PbI_3$ perovskite measured at various temperatures. The insets (c) and (d) show enlarged features of (a) and (b).

shown in Figure 2, obvious changes could be observed across the phase transitions, although some hysteresis was observed. The hysteresis is also seen in the samples stabilized at each temperature for over an hour, indicating that it is a long term effect. The tetragonal-orthorhombic phase transition occurs at approximately 156 K, while the orthorhombic-tetragonal phase transition temperature is circa 144 K.

The ellipsometry data at about 780 nm exhibits the most dramatic changes during phase changes, with Figure 3 showing the ellipsometry data at this wavelength plotted as a function of temperature. Obvious hysteresis behaviour could be observed during the cooling and heating cycles. This feature has also been reported for dielectric permittivity[22] and optical density[27] previously, while future work is required to verify the origin of this phenomenon. Notably, the ellipsometry data after this cooling-heating cycle are almost identical with original values confirming the optical properties after phase transitions are reversible.

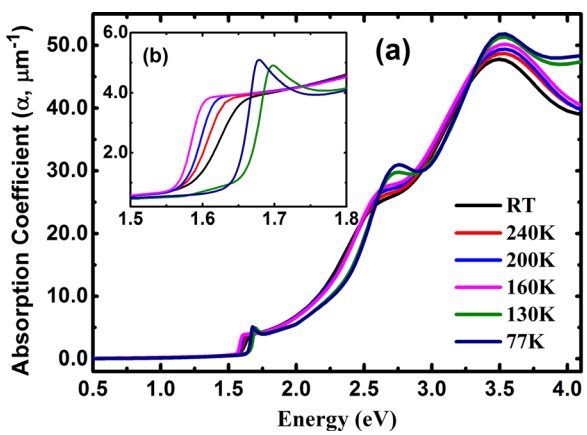

FIG. 5. Absorption coefficient of $CH_3NH_3PbI_3$ perovskite measured at various temperatures. The inset (b) shows enlarged features of (a) at the frequency range between 1.5 eV and 1.8 eV.

Temperature dependent real and imaginary dielectric functions were determined and are presented in Figure 4. The temperature of the sample was allowed to stabilize for approximately 1 h between measurements. Obvious evolutions of fundamental peaks could be observed as shown in the insets of Figures 4(a) and 4(b). Sharper peaks emerge in orthorhombic phases, which are attributed to stronger excitonic transitions.[28] A slight decrease in the dielectric constant could be observed with increasing temperature in each phase. This is consistent with the behaviour in other lead containing semiconductors like PbS, PbSe, and PbTe.[29]

The absorption coefficient, α, was calculated from the extinction coefficient k and is plotted in Figure 5(a). The direct bandgap at $E_0 = 1.61$ eV, and two absorption peaks at $E_1 = 2.5$ eV and $E_2 = 3.4$ eV (Refs. 30 and 31) are apparent in the absorption spectra. Consistent with previous reports, E_0 and E_2 transitions gradually shift towards higher energies as the temperature increases in each phase, whereas interestingly, the E_1 peak position was not as strongly shifted. A blue shift in the bandgap could be seen with increasing temperature in both the orthorhombic phase (77–130 K) and tetragonal phase (160–297 K).

To obtain a better understanding of energy band structures in $CH_3NH_3PbI_3$ perovskites, CP analysis was performed by fitting the second derivative spectra of the dielectric functions[32] by

$$\frac{d^2\varepsilon}{d\omega^2} = \begin{cases} n(n-1)Ae^{i\Phi}(\omega - E + i\Gamma), & n \neq 0 \\ Ae^{i\Phi}(\omega - E + i\Gamma)^{-2}, & n = 0, \end{cases} \quad (1)$$

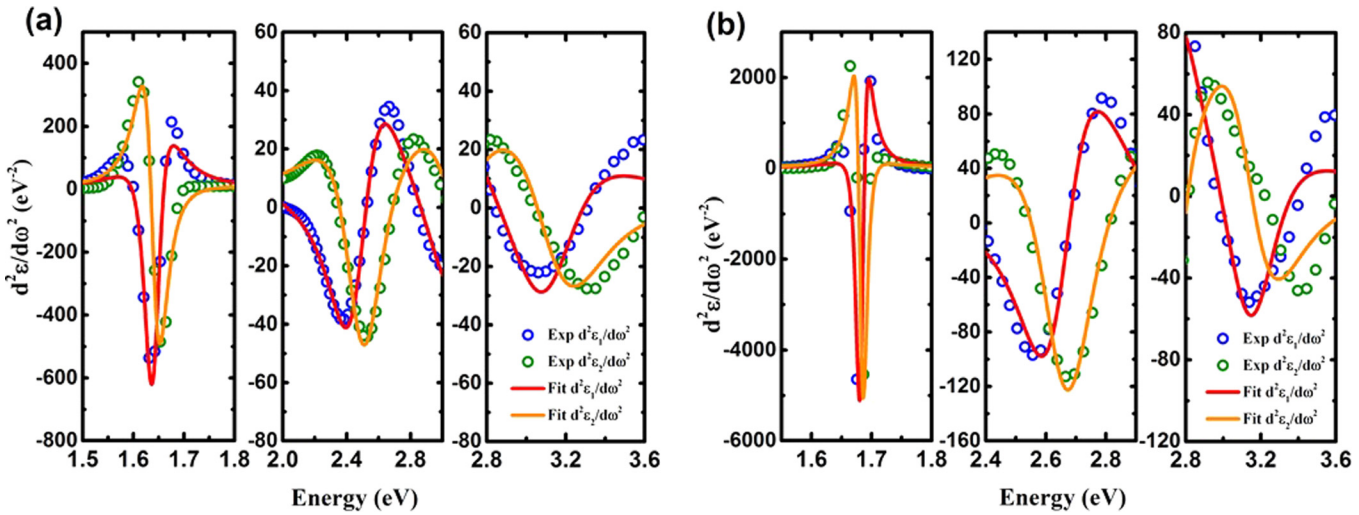

FIG. 6. Second derivatives of the real and imaginary parts of the dielectric function of $CH_3NH_3PbI_3$ perovskite measured as a function of energy at (a) room temperature and (b) 77 K. The experimental data is shown as open circles, while fitted values are plotted using solid lines.

TABLE I. Critical points of $CH_3NH_3PbI_3$ obtained by fitting the second derivatives of the real and imaginary parts of the dielectric function at different temperatures.

Temperature (K)	Critical point E_0 (eV)	Critical point E_1 (eV)	Critical point E_2 (eV)
77	1.681	2.657	3.144
130	1.697	2.643	3.295
160	1.596	2.553	2.955
200	1.608	2.556	3.043
240	1.625	2.542	3.073
298	1.639	2.487	3.115

TABLE II. Temperature coefficient $\partial E/\partial T$ of $CH_3NH_3PbI_3$ determined for tetragonal and orthorhombic phases.

Phases	Critical point E_0 (meV/K)	Critical point E_1 (meV/K)	Critical point E_2 (meV/K)
Orthorhombic	0.30	−0.26	2.85
Tetragonal	0.32	−0.49	1.10

where A, Φ, E, and Γ are the amplitude, excitonic phase angle, threshold energy and broadening of the peak, respectively. The exponent n is $-\frac{1}{2}$ for one dimensional, 0 for two dimensional or $\frac{1}{2}$ for three dimensional critical points. n equals -1 when describing excitonic optical transitions. In this analysis, $n=-1$ was used for all CP energies to account for the expected excitonic features (Figure 6).[20,33]

The critical points observed at E_0, E_1, and E_2 (Table I) agree well with the optical transitions previously assigned to excitations from the highest and second highest valence bands to the lowest conduction band split-off (E_0 and E_1) and from the doubly degenerate highest valence to the higher level split-off conduction band (E_2) in the Brillion zone of the cubic phase, respectively, that are reflected to the zone centre in the lower symmetry tetragonal and orthorhombic phases.[20,34]

As shown in Figure 7, the energies for critical points E_0, E_1, and E_2 vary almost linearly with temperature. As previously reported, commonly used models describing the temperature dependence of conventional semiconductors are no longer suitable for perovskite materials.[35] An obvious blue shift could be observed for E_0 and E_2 with increasing temperature, while E_1 shows a red, although smaller, shift. The band gap shift with temperature is principally associated with the combined effect of thermal expansion of the lattice and electron-phonon interaction.[36,37] The blue-shift of the first bandgap (i.e., E_0) in tetragonal and cubic phase has been recently shown to be due to the energy downshift of the conduction and valence band with temperature, with a higher strength for the latter.[38] The red-shift of E_1 still needs to be investigated. The temperature coefficient of E_0 determined for

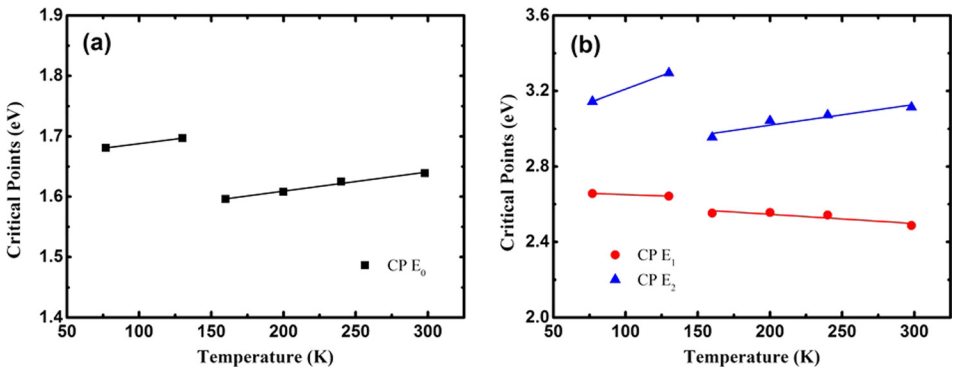

FIG. 7. Temperature dependence of the interband critical point energies of $CH_3NH_3PbI_3$ for tetragonal and orthorhombic phases.

the tetragonal phase $CH_3NH_3PbI_3$ of 0.32 meV/K is in good agreement with previously reported values (Table II).[33,35]

We have reported the temperature dependent optical properties of the $CH_3NH_3PbI_3$ perovskite in the range of 77 K to 297 K. The dielectric functions as well as interband critical points were determined in the 0.5–4 eV energy range. Increase in temperature results in a slight decrease in the dielectric constants for both orthorhombic and tetragonal phases. Critical point energies E_0 and E_2 show an obvious blue shift with increasing temperature, while E_1 is red-shifted.

The Australian Centre for Advanced Photovoltaics is supported by the Australian Government through the Australian Renewable Energy Agency (ARENA). The Australian Government does not accept responsibility for the views, information, or advice expressed herein. A.G. is grateful for support provided by the ARC Discovery DP140102003 Grant.

[1]M. A. Green, A. Ho-Baillie, and H. J. Snaith, "The emergence of perovskite solar cells," Nat. Photonics **8**(7), 506–514 (2014).
[2]N.-G. Park, "Perovskite solar cells: An emerging photovoltaic technology," Mater. Today **18**(2), 65–72 (2015).
[3]H. S. Jung and N.-G. Park, "Perovskite solar cells: from materials to devices," Small **11**(1), 10–25 (2015).
[4]M. A. Green and T. Bein, "Photovoltaics: Perovskite cells charge forward," Nat Mater. **14**(6), 559–561 (2015).
[5]S. Colella, E. Mosconi, P. Fedeli, A. Listorti, F. Gazza, F. Orlandi, P. Ferro, T. Besagni, A. Rizzo, G. Calestani, G. Gigli, F. De Angelis, and R. Mosca, "$MAPbI_{3-x}Cl_x$ mixed halide perovskite for hybrid solar cells: The role of chloride as dopant on the transport and structural properties," Chem. Mater. **25**(22), 4613–4618 (2013).
[6]C. S. Ponseca, T. J. Savenije, M. Abdellah, K. Zheng, A. Yartsev, T. Pascher, T. Harlang, P. Chabera, T. Pullerits, A. Stepanov, J.-P. Wolf, and V. Sundström, "Organometal halide perovskite solar cell materials rationalized: Ultrafast charge generation, high and microsecond-long balanced mobilities, and slow recombination," J. Am. Chem. Soc. **136**(14), 5189–5192 (2014).
[7]M. H. Du, "Efficient carrier transport in halide perovskites: Theoretical perspectives," J. Mater. Chem. A **2**(24), 9091–9098 (2014).
[8]A. Miyata, A. Mitioglu, P. Plochocka, O. Portugall, J. T.-W. Wang, S. D. Stranks, H. J. Snaith, and R. J. Nicholas, "Direct measurement of the exciton binding energy and effective masses for charge carriers in organic-inorganic tri-halide perovskites," Nat. Phys. **11**(7), 582–587 (2015).
[9]N. Onoda-Yamamuro, T. Matsuo, and H. Suga, "Calorimetric and IR spectroscopic studies of phase transitions in methylammonium trihalogenoplumbates," J. Phys. Chem. Solids **51**(12), 1383–1395 (1990).
[10]Y. Kawamura, H. Mashiyama, and K. Hasebe, "Structural study on cubic–tetragonal transition of $CH_3NH_3PbI_3$," J. Phys. Soc. Jpn. **71**(7), 1694–1697 (2002).
[11]T. Baikie, Y. Fang, J. M. Kadro, M. Schreyer, F. Wei, S. G. Mhaisalkar, M. Graetzel, and T. J. White, "Synthesis and crystal chemistry of the hybrid perovskite $(CH_3NH_3)PbI_3$ for solid-state sensitised solar cell applications," J. Mater. Chem. A **1**(18), 5628–5641 (2013).
[12]G. Xing, N. Mathews, S. S. Lim, N. Yantara, X. Liu, D. Sabba, M. Grätzel, S. Mhaisalkar, and T. C. Sum, "Low-temperature solution-processed wavelength-tunable perovskites for lasing," Nat. Mater. **13**(5), 476–480 (2014).
[13]J. M. Ball, S. D. Stranks, M. T. Horantner, S. Huttner, W. Zhang, E. J. W. Crossland, I. Ramirez, M. Riede, M. B. Johnston, R. H. Friend, and H. J. Snaith, "Optical properties and limiting photocurrent of thin-film perovskite solar cells," Energy Environ. Sci. **8**(2), 602–609 (2015).
[14]Q. Lin, A. Armin, R. C. R. Nagiri, P. L. Burn, and P. Meredith, "Electro-optics of perovskite solar cells," Nat. Photonics **9**(2), 106–112 (2015).
[15]C. W. Chen, S. Y. Hsiao, C. Y. Chen, H. W. Kang, Z. Y. Huang, and H. W. Lin, "Optical properties of organometal halide perovskite thin films and general device structure design rules for perovskite single and tandem solar cells," J. Mater. Chem. A **3**, 9152–9159 (2015).
[16]X. Ziang, L. Shifeng, Q. Laixiang, P. Shuping, W. Wei, Y. Yu, Y. Li, C. Zhijian, W. Shufeng, D. Honglin, Y. Minghui, and G. G. Qin, "Refractive index and extinction coefficient of $CH_3NH_3PbI_3$ studied by spectroscopic ellipsometry," Opt. Mater. Express **5**(1), 29–43 (2015).
[17]Y. Jiang, M. A. Green, R. Sheng, and A. Ho-Baillie, "Room temperature optical properties of organic–inorganic lead halide perovskites," Sol. Energy Mater. Sol. Cells **137**, 253–257 (2015).
[18]Y. Jiang, M. A. Green, R. Sheng, and A. Ho-Baillie, "Optical modelling data for room temperature optical properties of organic–inorganic lead halide perovskites," Data Brief **3**, 201–208 (2015).
[19]P. Löper, M. Stuckelberger, B. Niesen, J. Werner, M. Filipič, S.-J. Moon, J.-H. Yum, M. Topič, S. De Wolf, and C. Ballif, "Complex refractive index spectra of $CH_3NH_3PbI_3$ perovskite thin films determined by spectroscopic ellipsometry and spectrophotometry," J. Phys. Chem. Lett. **6**(1), 66–71 (2015).
[20]M. A. Green, Y. Jiang, A. M. Soufiani, and A. W.-Y. Ho-Baillie, "Optical properties of photovoltaic organic-inorganic lead halide perovskites," J. Phys. Chem. Lett. **6**, 4774–4785 (2015).
[21]A. Poglitsch and D. Weber, "Dynamic disorder in methylammoniumtrihalogenoplumbates (II) observed by millimeter-wave spectroscopy," J. Chem. Phys. **87**(11), 6373–6378 (1987).
[22]N. Onoda-Yamamuro, T. Matsuo, and H. Suga, "Dielectric study of CH_3NH_3PbX3 (X = Cl, Br, I)," J. Phys. Chem. Solids **53**(7), 935–939 (1992).
[23]C. Quarti, E. Mosconi, J. M. Ball, V. D'Innocenzo, C. Tao, S. Pathak, H. J. Snaith, A. Petrozza, and F. De Angelis, "Structural and optical properties of methylammonium lead iodide across the tetragonal to cubic phase transition: Implications for perovskite solar cells," Energy Environ. Sci. **9**, 155–163 (2016).
[24]F. Huang, Y. Dkhissi, W. Huang, M. Xiao, I. Benesperi, S. Rubanov, Y. Zhu, X. Lin, L. Jiang, Y. Zhou, A. Gray-Weale, J. Etheridge, C. R. McNeill, R. A. Caruso, U. Bach, L. Spiccia, and Y.-B. Cheng, "Gas-assisted preparation of lead iodide perovskite films consisting of a monolayer of single crystalline grains for high efficiency planar solar cells," Nano Energy **10**, 10–18 (2014).
[25]*Guide to using WVASE® 32* (J. A. Woollam Co., Inc., 2008).
[26]See supplementary material at http://dx.doi.org/10.1063/1.4941710 for fittings of experimental and modelled ellipsometry data of a $CH_3NH_3PbI_3$ perovskite film deposited on a glass substrate at 130, 160, 200, and 240 K.
[27]C. Wehrenfennig, M. Liu, H. J. Snaith, M. B. Johnston, and L. M. Herz, "Charge carrier recombination channels in the low-temperature phase of organic-inorganic lead halide perovskite thin films," APL Mater. **2**(8), 081513 (2014).
[28]V. D'Innocenzo, G. Grancini, M. J. P. Alcocer, A. R. S. Kandada, S. D. Stranks, M. M. Lee, G. Lanzani, H. J. Snaith, and A. Petrozza, "Excitons versus free charges in organo-lead tri-halide perovskites," Nat. Commun. **5**, 3586 (2014).
[29]J. N. Zemel, J. D. Jensen, and R. B. Schoolar, "Electrical and optical properties of epitaxial films of PbS, PbSe, PbTe, and SnTe," Phys. Rev. **140**(1A), A330–A342 (1965).
[30]M. Shirayama, H. Kadowaki, T. Miyadera, T. Sugita, M. Tamakoshi, M. Kato, T. Fujiseki, D. Murata, S. Hara, T. N. Murakami, S. Fujimoto, M. Chikamatsu, and H. Fujiwara, "Optical transitions in hybrid perovskite solar cells: Ellipsometry, density functional theory, and quantum efficiency analyses for $CH_3NH_3PbI_3$," Phys. Rev. Appl. **5**(1), 014012 (2016).
[31]A. M. A. Leguy, P. Azarhoosh, M. I. Alonso, M. Campoy-Quiles, O. J. Weber, J. Yao, D. Bryant, M. T. Weller, J. Nelson, A. Walsh, M. van Schilfgaarde, and P. R. F. Barnes, "Experimental and theoretical optical properties of methylammonium lead halide perovskites," Nanoscale (published online 2015).
[32]P. Lautenschlager, M. Garriga, L. Vina, and M. Cardona, "Temperature dependence of the dielectric function and interband critical points in silicon," Phys. Rev. B **36**(9), 4821–4830 (1987).
[33]A. M. Soufiani, F. Huang, P. Reece, R. Sheng, A. Ho-Baillie, and M. A. Green, "Polaronic exciton binding energy in iodide and bromide organic-inorganic lead halide perovskites," Appl. Phys. Lett. **107**, 231902 (2015).
[34]J. Even, L. Pedesseau, and C. Katan, "Analysis of multivalley and multibandgap absorption and enhancement of free carriers related to exciton screening in hybrid perovskites," J. Phys. Chem. C **118**(22), 11566–11572 (2014).
[35]K. Wu, A. Bera, C. Ma, Y. Du, Y. Yang, L. Li, and T. Wu, "Temperature-dependent excitonic photoluminescence of hybrid organometal halide perovskite films," Phys. Chem. Chem. Phys. **16**(41), 22476–22481 (2014).
[36]Y. P. Varshni, "Temperature dependence of the energy gap in semiconductors," Physica **34**(1), 149–154 (1967).
[37]M. Baleva, T. Georgiev, and G. Lashkarev, "On the temperature dependence of the energy gap in PbSe and PbTe," J. Phys.: Condens. Matter **2**(13), 2935 (1990).
[38]B. J. Foley, D. L. Marlowe, K. Sun, W. A. Saidi, L. Scudiero, M. C. Gupta, and J. J. Choi, "Temperature dependent energy levels of methylammonium lead iodide perovskite," Appl. Phys. Lett. **106**(24), 243904 (2015).